Wind regime changes in the Euro-Atlantic region driven by Late-Holocene Grand Solar Minima

P. Harding[1*], C. Martin-Puertas[1*], J. Sjolte[2], A. A. Walsh[1], R. Tjallingii[3], C. Langdon[4], S. P. E. Blockley[1], A. Brauer[3,5], P. Langdon[4], A. M. Milner[1], R. Muscheler[2], M. Perez[1].

1. Centre for Quaternary Research, Department of Geography, Royal Holloway, University of London, Egham, Surrey, TW20 0EX, UK.
2. Department of Geology, Lund University, Lund, Sweden.
3. GFZ German Research Centre for Geosciences, Climate Dynamics and Landscape Evolution, Potsdam, Germany.
4. School of Geography and Environmental Science, University of Southampton, Southampton, SO17 1BJ, UK.
5. University of Potsdam, Institute of Geoscience, Potsdam, Germany.

***poppy.harding@rhul.ac.uk**

***celia.martinpuertas@rhul.ac.uk**

ORCID ID:

P. Harding: 0000-0002-2184-9455

C. Martin-Puertas: 0000-0002-1349-5669

J. Sjolte: 0000-0003-0870-5331

A. A. Walsh: 0000-0002-0194-0438

R. Tjallingii: 0000-0002-9723-3622

C. Langdon:

S. P. E. Blockley: 0000-0003-0712-2118

A. Brauer: 0000-0002-6655-9451

P. Langdon: 0000-0003-2724-2643

A. M. Milner: 0000-0001-6882-3992

R. Muscheler: 0000-0003-2772-3631

M. Perez:

Acknowledgements:

This study has been funded by the Royal Society (ref: DH150185, RGF\EA\180100) and Horizon 2020 (MSCA EU project 705633 – SYNC). AAW is funded by the Natural Environmental Research Council (NE/L002485/1). We thank Professor Anson Mackay (University College London) for his support with diatom identification. We thank four anonymous reviewers for their constructive comments on the manuscript.

Keywords: Solar Activity, Atmospheric Circulation, Varves, Diatoms, Climate Change.

Abstract:

Understanding atmospheric response to radiative forcing, including the intensity and distribution of wind patterns is critical as this might have important implications in the coming decades. Long-term episodes of reduced solar activity (i.e. Grand Solar Minima, GSM) have triggered rapid climate change in the past, recorded in proxy-based records, including varved sediments from Meerfelder Maar, Germany, where the Homeric GSM (~2800 years ago) was studied. This study reconstructs windy conditions during the same GSM from Diss Mere, another varved record in England, to support the solar-wind linkage in the North Atlantic-European region. We use diatoms as proxies for windiness and support the palaeolimnological and palaeoclimate interpretation with a multi-proxy approach, including sedimentological, geochemical, and biological (chironomids and pollen) evidence. The diatom assemblage documents a shift from *Pantocsekiella ocellata* dominance to *Stephanodiscus parvus and Lindavia comta*, indicating a shift to more turbulent waters from ~2767 ± 28, linked to increased windiness. This shift is synchronous with changes in ^{14}C production, linked to solar activity changes during the GSM. Both proxy records reflect a rapid and synchronous atmospheric response (i.e. stronger winds) at the onset and during the GSM in the North Atlantic and continental Europe. In order to test whether this solar-wind linkage is consistent during other GSMs and to understand the underlying climate dynamics, we analyse the wind response to solar forcing at the two study sites during the Little Ice Age, a period that includes several GSMs. For this, we have used a reconstruction based on a 1200-year-long simulation with an isotope-enabled climate model. Our study suggests that wind anomalies in the North Atlantic-European sector may relate to an anomalous atmospheric circulation in response to long-term solar forcing leading to north-easterlies modulated by the East Atlantic pattern.

Introduction:

Solar activity has trended toward weaker solar cycles in the last four decades. Solar Cycle (SC) 24 (2009-2020) was below-average and SC 25 is expected to be weak. The prediction of future cycles comes with high uncertainty and some studies have suggested that the Sun is approaching a Grand Solar Minima (GSM) (Lean et al. 1997; Maycock et al. 2015), while the Solar Cycle Prediction Panel suggests SC 25 (2021 ~ 2032) might be the end of the current weakening (Nandy 2021). Reductions in total solar irradiance may only have a small influence on average global surface temperature (Maycock et al. 2015), however, there has been a contemporaneous decrease in ultraviolet solar irradiance (Lean et al. 1997), which could influence Northern Hemisphere regional winter climate through top-down mechanisms modulating modes of climate variability (Matthes et al. 2006; Woollings et al. 2010; Gray et al. 2010; Ineson et al. 2015). In northern-central Europe, persistent low solar activity is likely associated with anomalously cold winters on multidecadal timescales (Ineson et al. 2015) and tropospheric blocking events, likely associated with a more negative Arctic Oscillation index (Maycock et al. 2015), in the absence of other controlling factors. Long-term solar forcing does not, however, have an impact on North Atlantic Oscillation (NAO) (Ortega et al. 2015; Maycock et al. 2015), but instead, the East Atlantic pattern (EA) (Sjolte et al. 2018), the secondary mode of atmospheric circulation in the North Atlantic region. On the other hand, reanalysis data suggest wind speeds over western Europe are affected by the EA modulating the influence of the NAO (westerlies) on regional wind patterns (Zubiate et al. 2017). Thus, when NAO and EA have opposite indices there are positive wind anomalies over Ireland, the UK and central Europe (Zubiate et al. 2017). As such, decadal-scale variations of surface wind may be influenced by the variability in the dominant spatial climate patterns in the region, which define the main climate modes, for example the NOA, EA and Scandinavian pattern, Atlantic Multidecadal Variability (Zeng et al. 2019; Hernández et al. 2020). In addition, statistical models for wind series of the last 40 years reveal a reversal in global terrestrial stilling since 2010, with potentially significant impacts for Europe (Zeng et al. 2019). This decadal-scale shift to a positive trend of observed surface wind speeds coincides with the weak SC 24 and 25, suggesting enhanced windiness could continue, at least, for the next decade.

GSMs occur on centennial timescales (Usoskin et al. 2007), with the best studied (Dalton, Maunder, Spörer and Wolf Minima) occurring during the Little Ice Age (LIA, AD 1300 - 1850) (Brehm et al. 2021), a period also characterised by high volcanic activity (Miller et al. 2012). Annually resolved ^{14}C based reconstructions of solar reconstructions are now available for earlier GSM's, specifically the Wolf (1279-1349 AD) and Oort Minima (1021-1060AD) (Brehm et al. 2021). GSM are thought to potentially trigger notable cooling, particularly in Europe and North America (Owens et al. 2017), although evidence for the climatic impact of GSM is complicated by other factors, such as human modification of the environment and volcanic forcing (Sigl et al. 2015). One important GSM prior to the last millennia was the Homeric Minimum, which occurred ~2800 years ago (Stuiver and Kra 1986). It is not associated with significant volcanic forcing (Zielinski and Mershon 1997), and has much less human impact, that may influence climate proxy data. The period around the Homeric Minimum (~2800-2550 cal. BP) is divided into a higher amplitude initial event from ~2750-2635 cal. BP, that we consider as the Homeric GSM, followed by a lower amplitude, secondary minimum between 2614 – 2594 cal. BP (Reimer et al. 2020). Additionally, it must be noted that at ~2610 cal. BP there is a short-lived solar proton event, which triggered increased ^{14}C production (Muscheler et al. 2005; O'Hare et al. 2019; Reimer et al. 2020), however, this short-lived event is likely not linked to longer-term changes in solar activity. LIA climatic reconstructions from proxies and climate simulations report temperature and/or precipitation anomalies linked to low solar activity (Luterbacher 2001; Luterbacher et al. 2001; Shindell et al. 2001; Mauquoy et al. 2002). However, assessing past GSM influences on atmospheric changes, including wind intensity, duration, and direction, requires highly resolved wind-sensitive records with annual to decadal resolution. The annually laminated (varved) record from Meerfelder Maar, Germany (MFM; 50° 6'N, 6° 45'E) (Fig. 1.a) is a relatively rare record for this time period in Europe, showing increased windiness for 199 ± 9 varve years, coincident with the Homeric GSM (Martin-

Puertas et al. 2012). This study suggested top-down mechanisms triggered a synchronous in-phase response of atmospheric circulation to solar forcing (Martin-Puertas et al. 2012). However, the use of a single site only provides evidence of the impact of the GSM in one continental location and requires confirmation by additional highly resolved records, to allow the testing of the regional expression of GSM and to preclude a coincidental relationship.

This new study presents a multiproxy record from the varved sediments of Diss Mere (52° 22'N, 1° 6'E), with the main goal of testing the hypothesis of a comparable solar-induced shift in windiness in the British Isles during the Homeric GSM. The multiproxy study is built around a diatom-based reconstruction of Diss Mere sediments. Diatoms are sensitive to a range of environmental variables and can respond rapidly to changes in environmental conditions due to their short life cycles (hours to days), making them excellent palaeoecological, palaeoenvironmental and palaelimnological proxies (Kilham et al. 1986; Rioual et al. 2007; Jones 2013). While they are used in a diverse range of studies, one way diatoms can be employed is to infer changes in windiness, due to the specific requirements of some species (often smaller, less silicified taxa) for still, clear waters, while others (often larger and heavily silicified species) require turbulent waters to remain suspended within the photic zone (high light zone allowing phytoplankton to photosynthesise). Other species can thrive in conditions with reduced light and higher nutrient concentrations, generated as nutrients are resuspended in the water column from deeper mixing due to increased turbulence, and in some cases, it is documented that this can increase nutrient uptake (Kilham et al. 1986; Bradbury et al. 2002; Rioual et al. 2007; Winder and Hunter 2008; Dell'aquila et al. 2017). This means periods of change in wind and turbulence can be rapidly identified in the diatom assemblages. Our diatom record is supported by additional proxies; in this case, sedimentary data (varve counting, micromorphology and high resolution XRF analyses)(Martin-Puertas et al. 2012), combined with pollen analyses at the same resolution as the diatom reconstruction, to assess for landscape change and human impact, and a chironomid-inferred summer temperature record (C-IT). Together these allow reconstruction of climate and environment around the

Homeric GSM (2400 – 3000 cal. BP). This multiproxy approach is essential to ensure changes in the diatom reconstruction are not driven by changes on the landscape (e.g. landscape clearance removing shelter from the edge of the lake leading to detrital input into the lake, as this could also influence diatom productivity). We compare these to the wind sensitive MFM record, to produce a regional picture of the atmospheric circulation, and consider this in the light of published records of atmospheric change at this time, such as precipitation and aridity. We also examine a wind reconstruction that utilises seasonal ice core records and an isotope enabled model simulation during the LIA (Sjolte et al. 2018), which allows us to better understand the atmospheric response to GSM during the last millennium and support the climate response further back into the Holocene**.**

Study Site:

Diss Mere is a small eutrophic lake (~3.4 ha) located in the east of England (52° 22'N, 1° 6'E; 29 m a.s.l), on the edge of the North Sea (Fig. 1.a), a key region for wind energy production (Geyer et al. 2015). The lake is one of the few varved (annually-laminated) records in the UK covering the Holocene period, has a maximum water depth of ~6 m and no surface inflows or outflows (Peglar et al. 1984). Historic weather data for Norfolk show mean annual temperatures of 14.1°C max and 6.0°C min, mean annual precipitation of 652 mm (min rainfall February, max rainfall October), with seasonal average rainfall between 34 and 72 mm. Winds are predominantly from the south-east, with an average annual speed of 8.9 knots (10 m heights) (UK Met Office).

The sedimentary record (DISS-16) is ca. 14.5 m long and 8473 ± 40 varves are preserved between 8.88 – 13.15 m sediment depth. The varves consist of a calcite summer sub-layer and an organic-diatom autumn to spring sub-layer (Fig. 1.b) (Martin-Puertas et al. 2021). The floating varve chronology was tied to the IntCal20 timescale (Reimer et al. 2020), using a Bayesian *P_Sequence* deposition model with a fixed K and automatic outlier detection (Bronk Ramsey 2008, 2009). The model combined prior data from five radiocarbon dates and two known tephra layers (Glen Garry and OMH-185) (Martin-Puertas et al. 2021; Walsh et al.

2021). The resulting age-depth model (DISSV-2020) places the varved sequence between ca. 2100 and 10,300 cal. BP with decadal scale age uncertainties (95% confidence). The DISSV-2020 chronology was published by (Martin-Puertas et al. 2021) and further details on the construction of the chronology and a full dataset is freely available on the Varved Sediments Database (VARDA) repository at https://varve.gfz-potsdam.de/.

Data and Methods

Sediments and X-ray Fluorescence (XRF) core scanning data

Four parallel sediment cores were obtained in September 2016 from the deepest part of Diss Mere, using a 90 mm diameter UWITEC piston corer (Martin-Puertas et al. 2021). The sediment profiles were cross correlated using a total of 67 macroscopically visible marker layers and the best-preserved sections were combined to construct a 14.5 m long continuous composite profile (DISS-16) (Martin-Puertas et al. 2021). Varve counting and microfacies analysis (varve composition and varve thickness measurements) were studied on overlapping thin sections of 10 cm length under the microscope (x80 magnification). The duration of the climatic anomaly was calculated using the varve count-based time scale and relative varve counting error between marker layers. The uncertainty was calculated as the standard deviation of four replicate varve-counts. When we compare the duration of climate anomalies between Diss Mere varves and other varved records, the errors are propagated using the law of combination of errors (for more information see Supplementary Information).

Micro-XRF core scanning data were acquired every 0.2 mm by irradiation of the split core surface with a Cr X-ray source (30 kV, 30 mA) for 10 s using an ITRAX XRF-core scanner. XRF measurements are presented as central log ratios (clr) in order to provide a more reliable prediction of element concentration in the sediments (Weltje and Tjallingii 2008). Additional micro-XRF scanning maps were measured on impregnated sediment blocks used for thin-section preparation (Supplementary Fig. S1). Elemental mapping analyses were performed in a vacuum chamber at 50 µm resolution with a M4 Tornado micro-XRF scanner. This micro-XRF scanner is equipped with a Rh X-ray source (50 kV, 0.60 mA) in combination with polycapillary X-ray optics, to produce a high intensity irradiation spot of about 20 µm that allows fast measurement times (30 ms).

Diatoms

81 contiguous samples at 0.5 cm intervals between 909.3-949.8 cm were prepared for diatom compositional analyses following the digestion procedure (Battarbee et al. 2001). This involved removal of organics and carbonates with H_2O_2 and HCl respectively, and during rinses NH_3, was used to prevent diatom clumping. Diluted samples were pipetted onto cover slips, evaporated and then mounted in Naphrax™ mounting resin. Slides were counted using a Leitz Laborlux D at x1000 magnification, until a minimum of 300 diatoms were identified. Identifications were made using key diatom taxonomies (Krammer, K. and Lange-Bertalot 1986, 1988, 1991a, b; Lange-Bertalot 2001; Krammer 2002). Raw counts were transformed to percentages to provide relative abundances.

Pollen

For pollen analysis, 72 samples were taken contiguously at 0.5 cm resolution between 913.8 cm and 950.3 cm. Preparation followed well-established procedures (Faegri and Iversen 1989; Moore et al. 1991), with steps including the addition of *Lycopodium* spores before chemical treatment to enable the calculation of pollen concentrations (Stockmarr 1971), heavy liquid flotation using sodium polytungstate (SPT; at a specific gravity of 2.0 g cm^{-3}) and acetolysis. Slides were mounted in glycerine jelly and pollen identification took place under 400x magnification on an Olympus CX41 light microscope. A minimum counting sum of 500 Total Land Pollen (TLP) was achieved for each slide with pollen nomenclature following (Stace 2010).

Chironomidae

21 samples were taken between 909.8 and 950.3 cm, at a 2 cm resolution. Pilot samples had low head capsule concentrations, so sample volumes were increased (2.2 g for pilot samples, 10 g for additional samples). Samples were heated to 80°C in 10% KOH for 3 minutes or until

fully disaggregated and sieved through 180 µm and 90 µm meshes. Both size fractions were retained and agitated for 10-15 seconds in a sonic bath and re-sieved prior to picking and examined at x20 and x30 magnification. Chironomid remains were picked and mounted in hydromatrix on microscope slides, and identified to genus, sub-genus or species-type under x100-400 magnifications (Weiderholm 1983; Brooks et al. 2007). Percentages were calculated and diagrams plotted using Tilia and Tilia View (Grimm 1987). Mean July air temperatures were derived using the modern Norwegian chironomid–temperature transfer function (Brooks and Birks 2001) and percentage data are square root transformed prior to analyses, to minimise variance. Reconstructed temperatures were calculated using a weighted averaging partial least squares regression model (WA-PLS) and all analyses were run in R v 3.6.0 (R Core Team 2020).

Solar forcing record

Here we use the recently updated IntCal20 ^{14}C calibration curve (Reimer et al. 2020) to assess solar variability over the considered period. On timescales shorter than 500 years, the cosmogenic radionuclide variability is likely dominated by the effects of solar shielding of galactic cosmic rays, as illustrated by the agreement between higher ^{14}C production rate and lower solar activity over the past 400 years (Lal and Peters 1967; Snowball and Muscheler 2007; Muscheler et al. 2016). The agreement between ^{14}C production rate and ^{10}Be measured in Greenland ice cores supports the production-induced changes in these records, i.e. rejecting the hypothesis that the ^{14}C variations are driven by carbon cycle changes (Vonmoos et al. 2006). We calculated the ^{14}C production rate from the atmospheric ^{14}C fluctuations using a box-diffusion carbon cycle model (Siegenthaler 1983) assuming a constant carbon cycle. The uncertainty in the IntCal20 calibration curve was quantified using 100 posterior realizations of possible atmospheric ^{14}C curves obtained via fitting Bayesian splines to the ^{14}C data underlying IntCal20 (Reimer et al. 2020; Heaton et al. 2020). In Figure 3 we show the average of 100 possible realisations of the production rate.

Climate reconstruction

In the wider discussion of our results, we use a published reconstruction of sea level pressure (SLP) (Sjolte et al. 2018) covering CE 1241-1970, as well as the corresponding 850 mb wind extracted using the same methods (Sjolte et al. 2018). The reconstructions are based on the analogue method selecting best matching years from the output of the ECHAM-wiso/MPIOM isotope enabled climate model (horizontal resolution, 3.75° x 3.75°) compared to seasonal resolution Greenland ice core oxygen isotope records. Using an ensemble approach, the mean of the 39 best matching years of the climate model fields (e.g., SLP), are used to make the reconstruction. Full details of the methods used for the reconstruction are given in Sjolte et al. (2018), and the reconstruction has been validated against reanalysis data (Sjolte et al. 2018, 2020). The analysis for the min-max anomalies in Figure 4 excludes years possibly impacted by volcanic eruptions (Sjolte et al. 2018).

The proxy-record of Diss Mere

The time window in this study covers ca. 2400 to 3000 cal. BP (varve number 367 - 988), which is 40 cm long (910 – 950 cm of depth) in the sedimentary record of Diss Mere (Fig. 1.c). The Bayesian age-depth model provides an absolute age uncertainty of between ± 27 and 33 years along the studied interval and the relative varve counting error is ± 8 years (Supplementary Table 1), providing exceptional absolute and relative precision for our palaeoecological reconstruction (Martin-Puertas et al. 2021).

Varves are, generally, well preserved along the studied time window with Varve Quality Index (VQI) of 3.48 (4 being outstanding varve preservation). Varve thickness variability is relatively constant through most of the study interval with an average varve thickness of 0.6 mm (Fig. 2.a). The main components of the varved sediments, i.e. authigenic calcite, diatom blooms and detrital background sedimentation, are represented by Calcium (Ca_{clr}), Silica (Si_{clr}) and Titanium (Ti_{clr}), respectively (Fig. 2.b-d; Supplementary Information Fig. 1). Sediment composition is quite stable along the entire episode with Ca being the most abundant element. Ti values are low suggesting that the detrital input into the lake is a minor process influencing lake deposition. Si values are associated with biogenic silica production, primarily from diatom blooms occurring within the lake (Supplementary Information Fig. 1). Only a 60-year interval (ca. 2810 – 2750 cal. BP) at 936.4-929 cm depth show anomalies in both varve preservation and thickness from 2810 to 2750 cal. BP. For the first 40 years, from ca. 2810 to 2770 cal. BP, the varve thickness increases (average 0.93 mm) and both the calcite and the detritus sub-layer are thicker, but the laminations are discontinuous, which prevent an exhaustive varve thickness measurement (Fig. 2.a). The VQI goes down to a minimum of 2 during this interval. Varves are intercalated with 1-2 cm thick massive deposits mainly composed of Ca and Si that could represent re-deposition of calcite mud, likely from the littoral zone (Supplementary Fig. S1). From 2770 to 2750 cal. BP, the laminations are not well preserved (VQI=1) and 20 varves were interpolated (Fig. 1.c; Fig. 2.a; Supplementary Table S1). Following these 20 years, varves preserve well again (VQI=3-4) (Fig. 1.c; Fig. 2.a).

<u>Diatoms as a proxy record of windiness at Diss Mere</u>

Diatoms are abundant throughout the Diss Mere sequence, and during the studied time window are dominated by planktonic *Pantocsekiella ocellata* (Pantocsek) K. T. Kiss and E. Ács, *Lindavia comta* (Kützing) Nakov, Gullory, Julius, Theriot & Alverson, *Stephanodiscus parvus* Stoermer and Håk and littoral *Nitzschia gracilis* Hantzsch. The record divides into three main sections, with additional small fluctuations occurring throughout the assemblage. Diatom preservation is good at Diss Mere, as measured by the *F*_index (Fig.2.E; Supplementary Section 1.1), which has reasonably high values throughout (average 72% pristine), indicating the majority of diatom frustules preserved are in excellent condition. Although dissolution is generally limited, it is noted between 2748 - 2712 ± 28 cal. BP that the *F*_index values are lower, highlighting that during this period it is possible that some of the smaller and lightly silicified species may have been preferentially removed from the record. This is supported by lower levels of Si_{clr}, which may be linked to this increased diatom dissolution. This increased dissolution is likely due to lower silica saturation in the water column at this time (Cohen 2003; Flower and Ryves 2009). It is only once silica levels are restored, that the diatom *F*_Index values increase, due to increased silica availability.

The earliest section (~3000 cal. BP) of the Diss Mere diatom assemblage is relatively stable, with *P. ocellata* dominating (~50-90%), alongside lower (generally <30%), fluctuating *L. comta* and *N. gracilis*. *P. ocellata*'s dominance is linked to its opportunistic tendencies, small size and slow sinking rates, allowing it to thrive in wide-ranging conditions (Rioual et al. 2007; Malik and Saros 2016) (Supplementary Table S2). It's occurrence alongside *N. gracilis*, indicates high light intensity, which these species favour (Fritz 1989; Malik and Saros 2016), and consequently, that the period of mixing is limited (as this would reduce water clarity and light availability through sediment resuspension), but sufficient to allow low quantities of *L. comta* to be sustained in the plankton. A brief occurrence of *S. parvus* at ~2926 ± 28 cal. BP may indicate a short-lived period with increased mixing/turbulence, required by *Stephanodiscus* to sustain its position in the photic zone (Kilham 1990) (Supplementary Tables S2 and S3).

A second shift from *P. ocellata* to *S. parvus* between ~2767 - 2755 ± 28 cal. BP also indicates increased turbulence (triggering declining light availability due to reduced water clarity, needed for photosynthesis (Kilham et al. 1986; Kilham 1990; Bradbury et al. 2002; Rioual et al. 2007)) and littoral input, potentially from wind-induced wave activity at the shoreline, which may have driven the increased quantity of *N. gracilis* at this point (Fritz 1989). Deeper and prolonged annual mixing episode(s) could also explain the changes in the varve preservation during this period, where varves are interpolated, as varve preservation requires anoxic/suboxic bottom water (Zolitschka et al. 2015).

The following shift to *L. comta* at ~2749 ± 28 cal. BP is considered to indicate changing proportions of nutrients in the water column, potentially driven by a reduction in mixing depth and therefore reduced internal mixing of nutrients, including phosphorous, which *Stephanodiscus* requires in high quantities (Kilham et al. 1986; Kilham 1990; Rioual et al. 2007) (Fig. 2.f; Supplementary Fig. S1; Supplementary Table S2), although it still suggests continuing turbulence, which is required to keep it suspended in the photic zone (Winder and Hunter 2008). Low levels of *P. ocellata* are likely sustained during a shortened period of summer stratification (Rioual et al. 2007). Reduced mixing depth or duration may also explain the renewed varve preservation after ~2750 cal. BP. Alongside this, *N. gracilis* almost disappears from the record at ~2754 ± 28 cal. BP, indicating that light intensity is reduced (Fritz 1989), supporting the interpretation of increased turbulence (Supplementary Table S2). From 2621 ± 29 cal. BP *L. comta* completely disappears from the record, while *P. ocellata* returns to dominance, indicating reduced turbulence and wind induced mixing (Fig. 2.f; Supplementary Tables 2 and 3).

In summary, we suggest the occurrence of *L. comta* and *S. parvus* indicate increased turbulence in the lake and consider this a proxy for increased windiness in the area around the site (Moreno-Ostos et al. 2009)(Fig. 3a).

<u>Multi-proxy cross-validation of the climate signal</u>

In addition to the diatom record, we have included a ~5-year-resolution pollen record and a ~30 - 50-year-resolution chironomid inferred temperature reconstructions (CI-T), in order to reconstruct the landscape around the lake and to determine the extent to which land-use change could have impacted our proxy responses during this time interval. Arboreal taxa, such as *Quercus*, *Corylus* and *Alnus*, are well represented in the Diss Mere pollen profile, and abundances of these woody taxa remain relatively stable throughout (Fig. 1.h; Supplementary Fig. S1). Low levels of herbaceous taxa are present in the pollen record, and include taxa associated with human activity. Overall, we interpret the landscape at Diss Mere to comprise a vegetation mosaic of predominantly mixed-deciduous woodland with patches of open land. There is no evidence for widespread clearance of woodland cover during the interval presented (2988 – 2478 cal. BP), but the herbaceous taxa composition reflects the likely presence of some arable and pastoral activity in the vicinity of the lake. The Diss Mere pollen profile fits a pattern of low-impact, mixed pastoral arable landscape seen during the Late-Bronze Age in the UK (Brück 2019).

Given the high temporal resolution of the record, we see evidence of short-lived fluctuations in the relative abundance of woodland vs. open taxa between 2810 - 2770 cal. BP, indicating possible changes in the nature and intensity of the human activity. However, in this instance, if human activity did increase during this interval, it did not result in widespread woodland clearance around Diss Mere. We infer this from using the absolute pollen data (Fig. 1.h) that show the total amount of pollen from woodland taxa remained mostly stable, with mainly an increase in pollen from herbaceous taxa. A lack of evidence for large-scale woodland clearance suggests that small changes in vegetation would not have had a substantial impact on the lake system and ecology and functioning during this time interval, for example through erosion and associated detrital input from widespread land clearance. Therefore, we see no evidence for significant human impact on the lake during the study period, which support wind-forced turbulent conditions.

The CI-T data for the Diss Mere record highlight that during the early phase of our study interval (ca. 3000 - 2680 cal. BP), spring summer conditions remained warm, at least within the uncertainties of the technique, although it is possible that if the increased windiness highlighted from the diatoms is occurring during the autumn months, it may not be recorded by this predominantly summer proxy. However, from ~2680 cal. BP in the CI-T record it appears that even summer temperatures are reduced, with additional samples being required to confirm this in future (Fig. 2.g).

Atmospheric response to Late-Holocene long-term solar forcing in the European-Atlantic region.

Our Diss Mere diatom record shows a windiness anomaly from 2767 $\pm$ 28 cal. BP covering 147 ± 8 years, exactly coinciding with the GSM (Stuiver and Kra 1986) (Fig. 3). Due to the annual resolution of the GSM as measured in IntCal20 (Reimer et al. 2020), the maximum uncertainty of our correlation between the duration of our anomaly and the GSM is + 8.06 years. The record appears to show a winter response (i.e. autumn to spring) to solar forcing, when diatoms undergo their largest blooms during the mixing limnological season. However, the low solar activity might also have triggered summer cooling during the second half of the solar minimum as shown by the C-IT record (Fig. 2.g).

A climate change around the Homeric GSM has been widely reported around the world. In the North Atlantic-European region, there are some records that can be compared to our study to provide support for a regional climatic impact. Irish bog records have been used for a number of years to reconstruct bog wetness, and, by extension, precipitation. Multiple bog records for Ireland were synchronised using tephra horizons and this synchronisation showed a drying trend followed by a ‘wet shift’ between ~2800 and 2600 BP (Armit et al. 2014), with the wet shift occurring at the end of this period of atmospheric change. Furthermore, while chronological uncertainties, especially around the use of ‘wiggle matching’ for radiocarbon age modelling (Blockley et al. 2007), preclude detailed comparison with our results, a wet shift has also been reported during this period for the Netherlands (van Geel et al. 1996). Additionally, further to the south and east of our study, increased aridity has been reported for the Dead Sea between ~3000 and 2400 BP, based on varve counts and radiocarbon dating (Neugebauer et al. 2015). All these proxy records in this period suggest broader evidence for region wide changes in atmospheric dynamics.

The only other record with an annually-resolved wind reconstruction during the Homeric GSM linked to a robust chronology that is comparable to the Diss Mere record is MFM (Martin-Puertas et al. 2012). We compare these two records alongside cosmogenic isotope-based solar activity data (atmospheric ^{14}C production rates, ^{14}C) (Reimer et al. 2020) during the Homeric GSM (Fig. 3), to test potential solar-forced impacts on the wind patterns at the North Sea edge and western Europe. Both varved records report diatom proxies for wind strength (diatom composition, this study, and varve thickness linked to intensified diatom blooms in MFM (Martin-Puertas et al. 2012)). The onset of the windy conditions at Diss Mere occur very rapidly, in less than 5 varve years (based on the observed varve counts per/cm). It is important to note that the relative counting uncertainty in varve years, especially over short-lived events is always much smaller than the absolute uncertainty of placing those events into absolute calendar time. In this case the calendar age of the onset of windy conditions in Diss is 2767 ± 29 cal. BP, based on the Bayesian combination of varve counting, radiocarbon dating and tephrochronology that underpins the absolute chronology of the site (Martin-Puertas et al. 2021). This is synchronous with the onset of increased windiness in MFM which has an absolute age, based on varve counting and radiocarbon dating, of 2759 ± 39 cal. BP (Martin-Puertas et al. 2012). The combined absolute calendar uncertainty of the onset of the regional wind response is ± 48 years, which is also synchronous with the GSM at ~2750 cal. BP, reconstructed by the increase in ^{14}C production rates discussed above (Reimer et al. 2020). There are, however, important differences in the duration of the signals in the two varve records, with the wind anomaly lasting ~58 varve years longer in MFM (199 ± 9 varve years (Martin-Puertas et al. 2012)) than in Diss Mere (147 ± 8 varve years), and a combined varve year uncertainty of this comparison of + 12 varve years (Fig. 3; see supplementary for propagation of errors), suggesting different atmospheric responses across the GSM at these two locations. At Diss Mere, the end of the windy interval at 2638 ± 28 cal. BP, where diatom species switch back to dominance of *P. ocellata* from *L. comta*, which continues until the end of the studied interval (~2400 cal. BP). This switch in diatom dominance coincides with the end of the Homeric GSM at 2635 cal. BP (Reimer et al. 2020), while thicker varves continue in MFM until 2560 ± 48 cal. BP covering the secondary solar minimum at ~2614 - 2594 cal. BP (Fig. 3). According to the ^{14}C concentration changes observed in the IntCal20 curve (Reimer et al. 2020) (Fig. 3.d), this second solar minimum has a lower amplitude than the Homeric GSM, and may have had a less of an impact on atmospheric processes. Our initial interpretation of the comparison between the two records is that the Diss Mere record is more sensitive to the amplitude of solar forcing than MFM.

The relative proximity of MFM and Diss Mere (~1000 km distance) means it is logical to expect for the two sites to show similar changes. While this is clearly the case for the onset of the changes within the two records, the sustained turbulence signal at MFM compared to Diss Mere require further consideration. While the difference in duration between the two records could be down to chance and be driven by independent local factors, the co-occurrence of the shifts in the two diatom records lends support to a larger scale driver. We see coincidence as an explanation for the similarity of the two records as being unlikely for several reasons. Firstly, in MFM there is a direct record of the solar minimum in the sediment ^{10}Be profile that is absolutely in phase with the change in the diatom record. This places the onset of turbulent conditions synchronously with the solar forcing. Secondly, the fact that there is an identical switch, at the same time in Diss Mere, means this change is also synchronous with the annually resolved ^{14}C record of the solar minimum in IntCal20 (Reimer et al. 2020). To us, for all of this to line up randomly seems to be pushing chance too far as a likely explanation. Furthermore, while the diatom records do not allow quantitative reconstruction of wind speed, they do allow a qualitative estimation of windy conditions, independent between the sites, which suggests a strong relationship with external climate forcing. Future studies are now required on the few annually resolved records in the wider European region are needed to explore the relationship we propose between the amplitude of solar forcing and the dynamics of the atmospheric response across the region. Such records are very rare, however, other GSM's have available reconstructions of the influence of solar activity on atmospheric dynamics that are relevant to testing our interpretation.

Reconstruction of the wind response to long-term solar forcing in the last millennium

To examine whether the proxy-based linkage between windiness and GSM occurred during other GSMs in the Holocene and to provide additional context for interpreting the underlying feedback mechanisms, we use an atmospheric circulation reconstruction for winter (DJF) responses to solar forcing in the North Atlantic region, between 1241-1970 CE (Sjolte et al. 2018), with special emphasis on the wind patterns (Fig. 4; Fig. 5). We have chosen this time window because it covers the most recent period with GSMs, the LIA. Our reconstruction is the longest available from a very limited number of seasonally resolved atmospheric circulation reconstructions available for comparison (e.g. Luterbacher et al. 2002; Valler et al. 2021), with no such study existing for the Homeric GSM. While this is a different GSM, we argue that a large signal in solar forcing is required to see an impact in atmospheric circulation and, thus, this is the most meaningful comparison possible to consider alongside our proxy data.

It has been argued that 11-yr sunspot minima are correlated with negative index of the NAO, increased Atlantic/European blocking frequency (Gray et al. 2016) and weakness of the subpolar gyre (SPG) (Moffa-Sánchez et al. 2014), in response to the top-down mechanisms (Woollings et al. 2010). Atmospheric response to long-term solar forcing, however, resembles the EA (Sjolte et al. 2018) leading to a northwest-southeast gradient and intensified northerlies. At present, the EA is the secondary mode of climate variability in the North Atlantic with impact on western Europe but rarely on France and the UK (Barnston and Livezey 1987). During GSM, however, the long-term shift in atmospheric response is potentially due to an accumulative effect of atmosphere-ocean feedbacks over time in relation to a weaker SPG reducing the heat transport to the north-western North Atlantic and reinforcing, thus, mid-Atlantic blocking shifting atmospheric circulation from a westerlies-dominated circulation (NAO) to northeasterlies-dominated circulation (EA) (Sjolte et al. 2018). Our reconstruction results show anomalous northerlies (EA-like circulation) over the North Sea forced by GSM (Fig. 4.b), which agrees with a pronounced meridional circulation and reduced westerlies during the Late Maunder Minimum reported from ships' logbook daily wind records in the English Channel (Mellado-Cano et al. 2018).

As enhanced lake overturning could be sensitive to strong wind episodes rather than average wind strength, we have also analysed the correlation between the standard deviation (STD) of the 850 mb wind (i.e. wind strength) and solar forcing. These analyses were run for both the entire period of the reconstruction (1241-1970 CE) and a time window that includes the Spörer, Maunder and Dalton GSM during the LIA (1400-1970 CE) only, in order to assess potential spatial extension (i.e. westward displacement) of the meridional wind anomalies (i.e., EA-like circulation) linked to a shifting amplitude of the solar forcing (Fig. 5). The results suggest intensified winds at both MFM and Diss Mere occur during GSM, however, the signal appears to be expressed more consistently in western Europe than along the North Sea coast

(Fig. 5.a). A negative correlation at both sites is stable for the 1400-1970 CE time-window, but correlation is weaker between 1241-1400, a period of higher solar activity (Fig. 5.b), which indicates the wind strength signal is most closely associated with low solar activity (Supplementary Section 2). What is particularly interesting, is that for the full period of the reconstruction (1241-1970), which is a period with both solar minima, but also enhanced sunspot activity, the atmospheric response over Europe (including Diss Mere and MFM) is not significant (Fig. 4.a). Importantly, however, when we run for the model for time period covering the Spoorer and Maunder minimums (Fig. 5.a), when low solar activity is dominant, the atmospheric response to SLP is significant. Additionally, in terms of spatial distribution, the mapping of the reconstructed atmospheric response to solar forcing (Fig. 5.b) locates Diss Mere at the boundary between positive (west) and negative (east) wind-solar correlation zones, which would mark the western limit of the regions impacted by the EA-like circulation (Fig. 5.a).

Atmospheric dynamics and the spatial differences in wind response

Solar-forced spatial migrations of sea level pressure centres affecting the regional impact of the EA (Moffa-Sánchez et al. 2014; Hernández et al. 2020, 2021) could explain the absence of a wind response during the secondary solar minimum ~2614-2594 cal. BP in Diss Mere, while there is still a signal in MFM (Fig. 3). As suggested in Figure 5a, Diss Mere in the East of England is in a zone with lower correlation with long-term solar forcing than the region around MFM. Thus, while the EA was the principal mode of climate variability during the Homeric GSM as seen in both sites, the shorter solar minimum between ~2614-2594 cal. BP might not be of sufficient amplitude of solar forcing to keep an impact of the EA over the UK. Thus, the turbulence in the lake was not sufficient to maintain the dominance of *L. comta* and instead there is a return to *P. ocellata* which does not have the high nutrient requirements, and its smaller size allows it to thrive in less turbulent waters due to slow sinking rates (Cherepanova et al. 2010; Duleba et al. 2015; Malik and Saros 2016). However, caution is required, as Diss Mere and MFM are only separated by ~1000km and the SLP reconstruction has a resolution of 400km (Sjolte et al. 2018), so the difference between the two sites cannot be reproduced with absolute precision, however, and further testing of our evidence for the nature of wind regime change and GSM requires reconstructions with higher spatial resolution.

Conclusion

We have generated new wind sensitive proxy data from the high resolution annually laminated lake record at Diss Mere, Norfolk and compared this to annual wind sensitive proxies from MFM. Our data suggests that spatially transgressive changes may have occurred in the atmospheric response to GSMs, depending on the amplitude of the solar signal. Our study highlights the importance of understanding potential changes and regional variations in windiness (Lean et al. 1997; Maycock et al. 2015), for critical areas like the North Sea (Geyer et al. 2015). Further investigation is now required on the amplitude of the response of atmospheric circulation to long-term solar forcing and varying boundary conditions (i.e. orbital parameters, greenhouse gases concentration and feedback mechanisms). In particular, deepening our understanding of how solar-modulated modes of climate variability can trigger regional differences, which could have important influences on the spatial distribution of wind anomalies and impacts of extreme weather events, in the North Atlantic-European region (Zubiate et al. 2017).

Declarations

Funding: This study has been funded by the Royal Society (ref: DH150185, RGF\EA\180100) and Horizon 2020 (MSCA EU project 705633 – SYNC). A. A. Walsh is funded by the Natural Environmental Research Council (NE/L002485/1).

Conflicts of interest/Competing interests: The authors confirm there are no conflicts of interest/competing interests to declare.

Availability of data and material: Datasets available from Varved Sediments Database (VARDA) repository at https://varve.gfz-potsdam.de/.

Code availability: Not Applicable

Authors' contributions:

P. Harding and C. Martin-Puertas designed the study and led the writing of the manuscript. P. Harding was responsible for the diatom analyses. C. Martin-Puertas led the coring campaign and was responsible for sediment core data analyses and interpretation of the geochemical data. J. Sjolte was responsible for climate simulations. A. A. Walsh was responsible for the pollen analyses. R. Tjallingii ran the geochemical analyses and contributed to the interpretation of the data. CL and PL provided the C-IT data. P. Harding, C. Martin-Puertas, A. A. Walsh, M. Perez, R. Tjallingii, C. Langdon, P. Langdon, S. Blockley, A. Brauer and A. M. Milner jointly interpreted the proxy data and J. Sjolte, P. Harding, C. Martin-Puertas, S. Blockley and R. Muscheler jointly interpreted the climatic implications of the study. All the authors contributed to the discussion and the writing of the final manuscript.

Ethics approval: Not Applicable

References

Armit I, Swindles GT, Becker K, et al (2014) Rapid climate change did not cause population collapse at the end of the European Bronze Age. Proceedings of the National Academy of Sciences of the United States of America 111:17045–17049. https://doi.org/10.1073/pnas.1408028111

Barnston AG, Livezey RE (1987) Classification, seasonality and persistence of low-frequency atmospheric circulation patterns. Monthly Weather Review 115:1083–1126. https://doi.org/10.1175/1520-0493(1987)115<1083:CSAPOL>2.0.CO;2

Battarbee R, Juggins S, Gasse F, et al (2001) An Information System for Palaeoenvironmental Reconstruction. EDDI 81:1–94

Blockley SPE, Blaauw M, Bronk Ramsey C, van der Plicht J (2007) Building and testing age models for radiocarbon dates in Lateglacial and Early Holocene sediments. Quaternary Science Reviews 26:1915–1926. https://doi.org/10.1016/j.quascirev.2007.06.007

Bradbury P, Cumming B, Laird K (2002) A 1500-year record of climatic and environmental change in Elk Lake, Minnesota III: Measures of past primary productivity. Journal of Paleolimnology 27:321–340. https://doi.org/10.1023/A:1016035313101

Brehm N, Bayliss A, Christl M, et al (2021) Eleven-year solar cycles over the last millennium revealed by radiocarbon in tree rings. Nature Geoscience 14:10–15. https://doi.org/10.1038/s41561-020-00674-0

Bronk Ramsey C (2009) Dealing with outliers and offsets in radiocarbon dating. Radiocarbon 51:1023–1045. https://doi.org/https://doi.org/10.1017/S0033822200034093

Bronk Ramsey C (2008) Deposition models for chronological records. Quaternary Science Reviews 27:42–60. https://doi.org/https://doi.org/10.1016/j.quascirev.2007.01.019

Brooks SJ, Birks HJB (2001) Chironomid-inferred air temperatures from Lateglacial and Holocene sites in north-west Europe: Progress and problems. Quaternary Science Reviews 20:1723–1741. https://doi.org/10.1016/S0277-3791(01)00038-5

Brooks SJ, Langdon PG, Heiri O (2007) The identification and use of Palaearctic Chironomindae larvae in palaeoecology., QRA Techni. Quaternary Research Association, London

Brück J (2019) The character of Late Bronze Age settlement in southern Britain. The Earlier Iron Age in Britain and the Near Continent 24–38. https://doi.org/10.2307/j.ctvh1dwqj.4

Cherepanova M V., Usol'tseva M V., Pushkar VS, Dubrovina YuF (2010) Morphogenesis in Cyclotella ocellata — complex from Lake El'gygytgyn (Chukchi Peninsula) during the Pleistocene-Holocene. Paleontological Journal 44:1252–1261. https://doi.org/10.1134/S0031030110100035

Cohen AS (2003) Paleolimnology : the history and evolution of lake systems. Oxford University Press, Oxford, New York

Dell'aquila G, Ferrante MI, Gherardi M, et al (2017) Nutrient consumption and chain tuning in diatoms exposed to storm-like turbulence. Scientific Reports 7:. https://doi.org/10.1038/S41598-017-02084-6

Duleba M, Kiss KT, Földi A, et al (2015) Morphological and genetic variability of assemblages of *Cyclotella ocellata* Pantocsek/ *C. comensis* Grunow complex (Bacillariophyta, Thalassiosirales). Diatom Research 30:283–306. https://doi.org/10.1080/0269249X.2015.1101402

Ebisuzaki W (1997) A method to estimate the statistical significance of a correlation when the data are serially correlated. Journal of Climate 10:2147–2153. https://doi.org/10.1175/1520-0442(1997)010<2147:AMTETS>2.0.CO;2

Faegri K, Iversen J (1989) Textbook of Pollen Analysis., 4th edn. John Wiley and Sons Ltd, Chichester, UK

Flower R, Ryves D (2009) Diatom preservation: differential preservation of sedimentary diatoms in two saline lakes. Acta Botanica Croatia 68:381–399

Fritz SC (1989) Lake Development and Limnological Response to Prehistoric and Historic Land-Use in Diss, Norfolk, U.K. The Journal of Ecology 77:182. https://doi.org/10.2307/2260924

Geyer B, Weisse R, Bisling P, Winterfeldt J (2015) Climatology of North Sea wind energy derived from a model hindcast for 1958-2012. Journal of Wind Engineering and Industrial Aerodynamics 147:18–29. https://doi.org/10.1016/j.jweia.2015.09.005

Gray LJ, Beer J, Geller M, et al (2010) Solar Influences on Climate. Reviews of Geophysics 48:RG4001. https://doi.org/10.1029/2009RG000282

Gray LJ, Woollings TJ, Andrews M, Knight J (2016) Eleven-year solar cycle signal in the NAO and Atlantic/European blocking. Quarterly Journal of the Royal Meteorological Society 142:1890–1903. https://doi.org/10.1002/qj.2782

Grimm EC (1987) CONISS: a FORTRAN 77 program for stratigraphically constrained cluster analysis by the method of incremental sum of squares. Computers & Geosciences 13:13–35. https://doi.org/10.1016/0098-3004(87)90022-7

Heaton TJ, Blaauw M, Blackwell PG, et al (2020) The IntCal20 Approach to Radiocarbon Calibration Curve Construction: A New Methodology Using Bayesian Splines and Errors-in-Variables. Radiocarbon 62:821–863. https://doi.org/10.1017/RDC.2020.46

Hernández A, Cachão M, Sousa P, et al (2021) External forcing mechanisms controlling the North Atlantic coastal upwelling regime during the mid-Holocene. Geology 49:433–437. https://doi.org/10.1130/G48112.1

Hernández A, Sánchez-López G, Pla-Rabes S, et al (2020) A 2,000-year Bayesian NAO reconstruction from the Iberian Peninsula. Scientific Reports 10:14961. https://doi.org/10.1038/s41598-020-71372-5

Ineson S, Maycock AC, Gray LJ, et al (2015) Regional climate impacts of a possible future grand solar minimum. Nature Communications 6: 7535:1–8. https://doi.org/10.1038/ncomms8535

Jones VJ (2013) Diatom Introduction. In: Encyclopedia of Quaternary Science: Second Edition. Elsevier, pp 471–480

Kilham P (1990) Ecology of Melosira Species in the Great Lakes of Africa. Springer, Berlin, Heidelberg, pp 414–427

Kilham P, Kilham SS, Hecky RE (1986) Hypothesized resource relationships among African planktonic diatoms. Limnology and Oceanography 31:1169–1181. https://doi.org/10.4319/lo.1986.31.6.1169

Krammer K (2002) Diatoms of Europe. Diatoms of the European Inland Waters and Comparable Habitats. Volume 3: Cymbella. Germany

Krammer, K. and Lange-Bertalot H (1991a) Bacillariophyceae. 3: Teil: Centrales, Fragilariaceae, Eunotiaceae., Süßwasserf. Gustav Fischer Verlag, Stuttgart, Jena.

Krammer, K. and Lange-Bertalot H (1988) Bacillariophyceae. 2: Teil: Bacillariaceae, Epithmiaceae, Surirellaceae., Süßwasserf. Gustav Fischer Verlag, Stuttgart, New York.

Krammer, K. and Lange-Bertalot H (1986) Bacillariophyceae. 1: Teil: Naviculaceae., Süßwasserf. Gustav Fischer Verlag, Stuttgart, New York

Krammer, K. and Lange-Bertalot H (1991b) Bacillariophyceae. 4: Teil: Achnanthaceae., Süßwasserf. Gustav Fischer Verlag, Stuttgart, Jena.

Lal D, Peters B (1967) Cosmic Ray Produced Radioactivity on the Earth. Springer, Berlin, Heidelberg, pp 551–612

Lange-Bertalot H (2001) Diatoms of Europe: Diatoms of the Europe inland waters and comparable habitats. Volume 2: Navicula sensu stricto, 10 Genera separated from Navicula sensu lato, Frustulia. Germany

Lean JL, Rottman GJ, Kyle HL, et al (1997) Detection and parameterization of variations in solar mid- and near-ultraviolet radiation (200-400 nm). Journal of Geophysical Research Atmospheres 102:29939–29956. https://doi.org/10.1029/97jd02092

Luterbacher J (2001) The Late Maunder Minimum (1675–1715) — Climax of the ‘Little Ice Age’ in Europe. In: History and Climate. Springer US, pp 29–54

Luterbacher J, Rickli R, Xoplaki E, et al (2001) The Late Maunder Minimum (1675-1715) - A key period for studying decadal scale climatic change in Europe. Climatic Change 49:441–462. https://doi.org/10.1023/A:1010667524422

Luterbacher J, Xoplaki E, Dietrich D, et al (2002) Reconstruction of sea level pressure fields over the Eastern North Atlantic and Europe back to 1500. Climate Dynamics 2001 187 18:545–561. https://doi.org/10.1007/S00382-001-0196-6

Malik HI, Saros JE (2016) Effects of temperature, light and nutrients on five Cyclotella sensu lato taxa assessed with in situ experiments in arctic lakes. Journal of Plankton Research 38:431–442. https://doi.org/10.1093/plankt/fbw002

Martin-Puertas C, Matthes K, Brauer A, et al (2012) Regional atmospheric circulation shifts induced by a grand solar minimum. Nature Geoscience 5:397–401. https://doi.org/10.1038/ngeo1460

Martin-Puertas C, Walsh AA, Blockley SPE, et al (2021) The First Holocene Varve Chronology for the UK: based on the integration of varve counting, radiocarbon dating and tephrostratigraphy from Diss Mere (UK). Quaternary Geochronology 61:101134. https://doi.org/10.1016/j.quageo.2020.101134

Matthes K, Kuroda Y, Kodera K, Langematz U (2006) Transfer of the solar signal from the stratosphere to the troposphere: Northern winter. Journal of Geophysical Research Atmospheres 111:. https://doi.org/10.1029/2005JD006283

Mauquoy D, van Geel B, Blaauw M, van der Plicht J (2002) Evidence from northwest European bogs shows ‘Little Ice Age’ climatic changes driven by variations in solar activity. The Holocene 12:1–6. https://doi.org/10.1191/0959683602hl514rr

Maycock AC, Ineson S, Gray LJ, et al (2015) Possible impacts of a future grand solar minimum on climate: Stratospheric and global circulation changes. Journal of Geophysical Research: Atmospheres 120:9043–9058. https://doi.org/10.1002/2014JD022022

Mellado-Cano J, Barriopedro D, García-Herrera R, et al (2018) Euro-Atlantic atmospheric circulation during the Late Maunder Minimum. Journal of Climate 31:3849–3863. https://doi.org/10.1175/JCLI-D-17-0261.1

Miller GH, Geirsdóttir Á, Zhong Y, et al (2012) Abrupt onset of the Little Ice Age triggered by volcanism and sustained by sea-ice/ocean feedbacks. Geophysical Research Letters 39:1–5. https://doi.org/10.1029/2011GL050168

Moffa-Sánchez P, Born A, Hall IR, et al (2014) Solar forcing of North Atlantic surface temperature and salinity over the past millennium. Nature Geoscience 7:275–278. https://doi.org/10.1038/ngeo2094

Moore PD, Webb JA, Collinson ME (1991) Pollen Analysis. Blackwell Science Inc, Oxford

Moreno-Ostos E, Cruz-Pizarro L, Basanta A, George DG (2009) The influence of wind-induced mixing on the vertical distribution of buoyant and sinking phytoplankton species. Aquatic Ecology 43:271–284. https://doi.org/10.1007/s10452-008-9167-x

Muscheler R, Adolphi F, Herbst K, Nilsson A (2016) The Revised Sunspot Record in Comparison to Cosmogenic Radionuclide-Based Solar Activity Reconstructions. Solar Physics 291:3025–3043. https://doi.org/10.1007/s11207-016-0969-z

Muscheler R, Beer J, Kubik PW, Synal HA (2005) Geomagnetic field intensity during the last 60,000 years based on 10Be and 36Cl from the Summit ice cores and 14C. Quaternary Science Reviews 24:1849–1860. https://doi.org/10.1016/j.quascirev.2005.01.012

Nandy D (2021) Progress in Solar Cycle Predictions: Sunspot Cycles 24–25 in Perspective. Solar Physics 2021 296:3 296:1–27. https://doi.org/10.1007/S11207-021-01797-2

Neugebauer I, Brauer A, Schwab MJ, et al (2015) Evidences for centennial dry periods at ~3300 and ~2800 cal. yr BP from micro-facies analyses of the Dead Sea sediments. Holocene 25:1358–1371. https://doi.org/10.1177/0959683615584208

O'Hare P, Mekhaldi F, Adolphi F, et al (2019) Multiradionuclide evidence for an extreme solar proton event around 2,610 B.P. (~660 BC). Proceedings of the National Academy of Sciences of the United States of America 116:5961–5966. https://doi.org/10.1073/pnas.1815725116

Ortega P, Lehner F, Swingedouw D, et al (2015) A model-tested North Atlantic Oscillation reconstruction for the past millennium. Nature 523:71–74. https://doi.org/10.1038/nature14518

Owens MJ, Lockwood M, Hawkins E, et al (2017) The Maunder minimum and the Little Ice Age: an update from recent reconstructions and climate simulations. Journal of Space Weather and Space Climate 7:A33. https://doi.org/10.1051/swsc/2017034

Peglar SM, Fritz SC, Alapieti T, et al (1984) Composition and formation of laminated sediments in Diss Mere, Norfolk, England. Boreas 13:13–28. https://doi.org/10.1111/j.1502-3885.1984.tb00054.x

R Core Team (2020) R: A Language and Environment for Statistical Computing.

Reimer PJ, Austin WEN, Bard E, et al (2020) The IntCal20 Northern Hemisphere Radiocarbon Age Calibration Curve (0-55 cal kBP). Radiocarbon 62:725–757. https://doi.org/10.1017/RDC.2020.41

Rioual P, Andrieu-Ponel V, de Beaulieu J-LL, et al (2007) Diatom responses to limnological and climatic changes at Ribains Maar (French Massif Central) during the Eemian and Early Würm. Quaternary Science Reviews 26:1557–1609. https://doi.org/10.1016/j.quascirev.2007.03.009

Shindell DT, Schmidt GA, Mann ME, et al (2001) Solar forcing of regional climate change during the Maunder Minimum. Science 294:2149–2152. https://doi.org/10.1126/science.1064363

Siegenthaler U (1983) Uptake of excess CO2 by an outcrop-diffusion model of the ocean. Journal of Geophysical Research 88:3599–3608. https://doi.org/10.1029/JC088iC06p03599

Sigl M, Winstrup M, McConnell JR, et al (2015) Timing and climate forcing of volcanic eruptions for the past 2,500 years. Nature 523:543–549. https://doi.org/10.1038/nature14565

Sjolte J, Adolphi F, Vinther BM, et al (2020) Seasonal reconstructions coupling ice core data and an isotope-enabled climate model - Methodological implications of seasonality, climate modes and selection of proxy data. Climate of the Past 16:1737–1758. https://doi.org/10.5194/CP-16-1737-2020

Sjolte J, Sturm C, Adolphi F, et al (2018) Solar and volcanic forcing of North Atlantic climate inferred from a process-based reconstruction. Climate of the Past 14:1179–1194. https://doi.org/10.5194/cp-14-1179-2018

Snowball I, Muscheler R (2007) Palaeomagnetic intensity data: An Achilles heel of solar activity reconstructions. Holocene 17:851–859. https://doi.org/10.1177/0959683607080531

Stace C (2010) New Flora of the British Isles., 3rd edn. Cambridge University Press, Cambridge

Steinhilber F, Abreu JA, Beer J, et al (2012) 9,400 years of cosmic radiation and solar activity from ice cores and tree rings. Proceedings of the National Academy of Sciences 109:5967–5971. https://doi.org/10.1073/pnas.1118965109

Stockmarr J (1971) Tablets with spores used in absolute pollen analysis. Pollen et Spores 13:615–621

Stuiver M, Kra RS (1986) Calibration issue, Proceedings of the 12th International 14C conference. Radiocarbon 28:805–1030

UK Met Office Marham (Norfolk) UK climate averages - Met Office. https://www.metoffice.gov.uk/research/climate/maps-and-data/uk-climate-averages/u127sby66. Accessed 7 Oct 2021

Usoskin IG, Solanki SK, Kovaltsov GA (2007) Grand minima and maxima of solar activity: New observational constraints. Astronomy and Astrophysics 471:301–309. https://doi.org/10.1051/0004-6361:20077704

Valler V, Franke J, Brugnara Y, Brönnimann S (2021) An updated global atmospheric paleo-reanalysis covering the last 400 years. Geoscience Data Journal 00:1–19. https://doi.org/10.1002/GDJ3.121

van Geel B, Buurman J, Waterbolk HT (1996) Archaeological and palaeoecological indications of an abrupt climate change in The Netherlands, and evidence for climatological teleconnections around 2650 BP. Journal of Quaternary Science 11:451–460. https://doi.org/10.1002/(SICI)1099-1417(199611/12)11:6<451::AID-JQS275>3.0.CO;2-9

Vonmoos M, Beer J, Muscheler R (2006) Large variations in Holocene solar activity: Constraints from 10Be in the Greenland Ice Core Project ice core. Journal of Geophysical Research: Space Physics 111:. https://doi.org/10.1029/2005JA011500

Walsh AA, Blockley SPE, Milner AM, et al (2021) Complexities in European Holocene cryptotephra dispersal revealed in the annually laminated lake record of Diss Mere, East Anglia. Quaternary Geochronology 66:101213. https://doi.org/10.1016/J.QUAGEO.2021.101213

Weiderholm T (1983) Chironomidae of the Holarctic region. Keys and Diagnoses. Part I. Larvae., Entomologi. Swedish Research Council, Stockholm

Weltje GJ, Tjallingii R (2008) Calibration of XRF core scanners for quantitative geochemical logging of sediment cores: Theory and application. Earth and Planetary Science Letters 274:423–438. https://doi.org/10.1016/J.EPSL.2008.07.054

Winder M, Hunter DA (2008) Temporal organization of phytoplankton communities linked to physical forcing. Oecologia 156:179–192. https://doi.org/10.1007/s00442-008-0964-7

Woollings T, Lockwood M, Masato G, et al (2010) Enhanced signature of solar variability in Eurasian winter climate. Geophysical Research Letters 37:. https://doi.org/10.1029/2010GL044601

Zeng Z, Ziegler AD, Searchinger T, et al (2019) A reversal in global terrestrial stilling and its implications for wind energy production. Nature Climate Change 9:979–985. https://doi.org/10.1038/s41558-019-0622-6

Zielinski GA, Mershon GR (1997) Paleoenvironmental implications of the insoluble microparticle record in the GISP2 (Greenland) ice core during the rapidly changing climate of the Pleistocene-Holocene transition. Bulletin of the Geological Society of America 109:547–559. https://doi.org/10.1130/0016-7606(1997)109<0547:PIOTIM>2.3.CO

Zolitschka B, Francus P, Ojala AEK, Schimmelmann A (2015) Varves in lake sediments - a review. Quaternary Science Reviews 117:1–41

Zubiate L, McDermott F, Sweeney C, O’Malley M (2017) Spatial variability in winter NAO–wind speed relationships in western Europe linked to concomitant states of the East Atlantic and Scandinavian patterns. Quarterly Journal of the Royal Meteorological Society 143:552–562. https://doi.org/10.1002/qj.2943

Figures and Tables

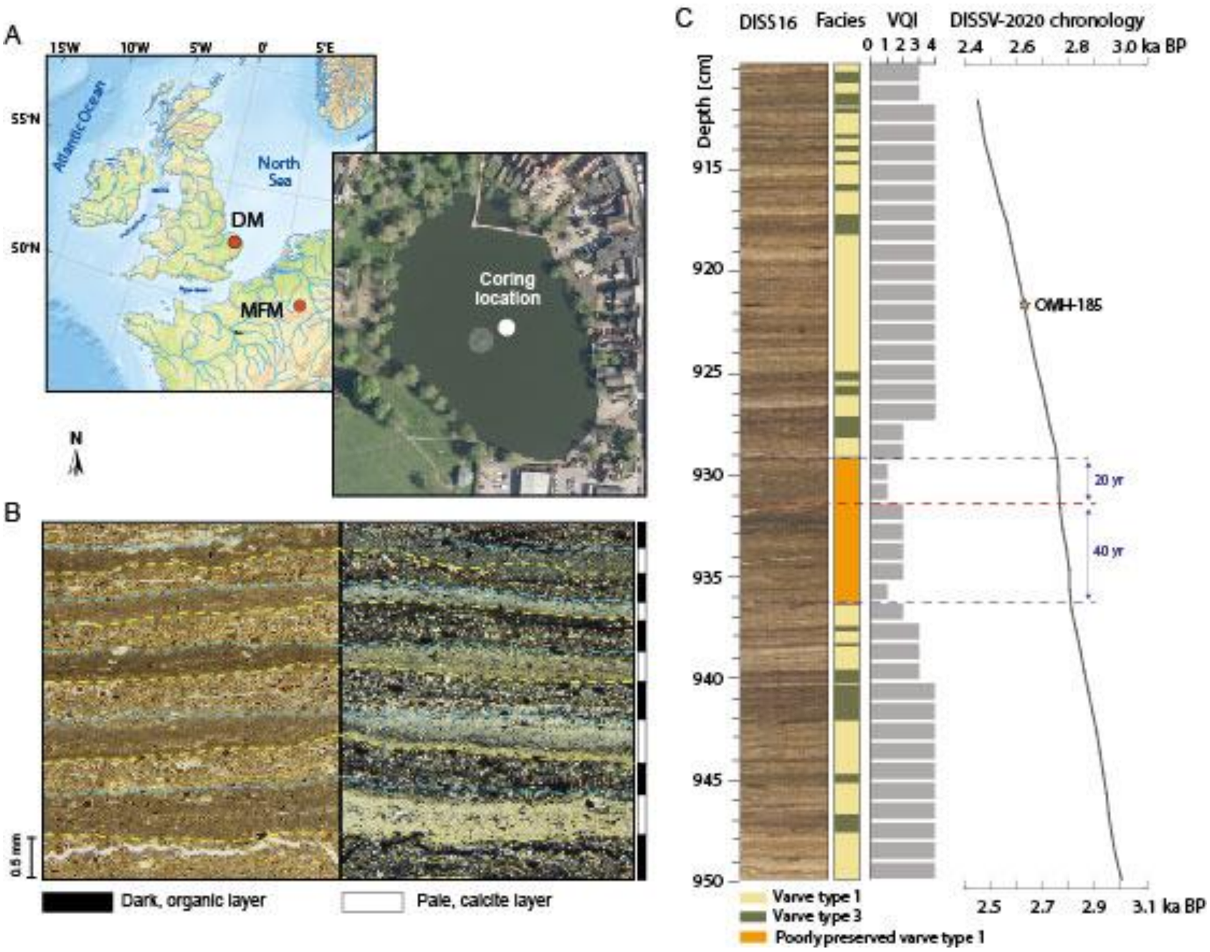

Fig. 1 Site Map and Diss Mere Proxy Records (A) European regional map showing Diss Mere, UK and Meerfelder Maar, Germany (MFM), alongside aerial photography of Diss Mere (B) Structure of varves in the Diss Mere record in plane light (left) and in polarized light (right): dark organic varves (primarily planktonic diatoms, organic, mostly aquatic, matter and a low amount of detrital sediments) and calcite varves made of a pale spring/summer sub-layer (primarily planktonic diatoms and authigenic calcite), (C) Diss 16 core stratigraphy and facies alongside Varve Quality Index (VQI) and the DISSV-2020 chronology for the studied interval (Martin-Puertas et al. 2021).

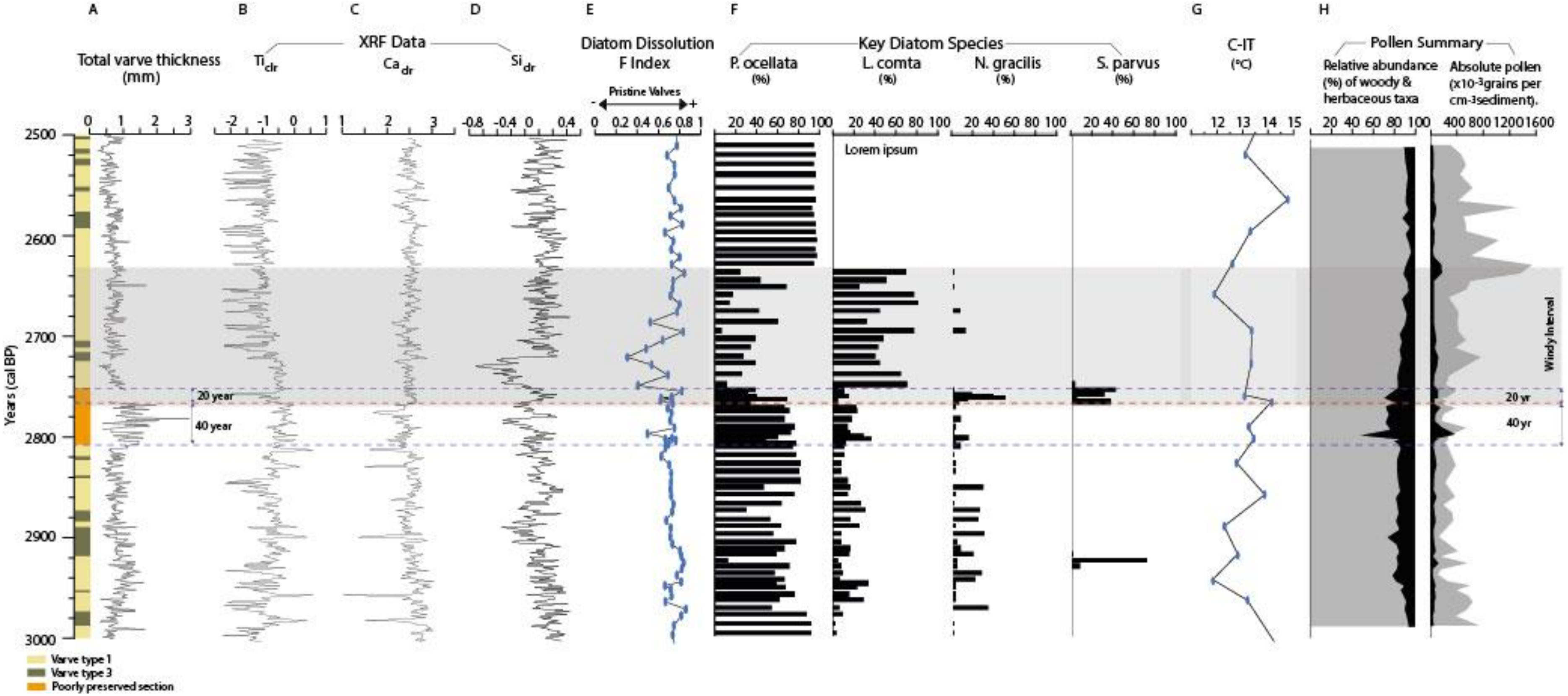

Fig. 2 Diss Mere sediment and proxy records for the study interval, 910-950 cm of sediment depth. From left to right: (A) Diss Mere Microfacies - varve type 1 corresponds to a calcite (spring-summer) / diatomaceous detritus (autumn-winter) couplet and varve type 3 corresponds to a diatom bloom (spring-summer) / diatomaceous detritus (autumn-winter)(Martin-Puertas et al. 2021) alongside total varve thickness (mm); (B-D) XRF Data (B) Ti central logged ratio; (C) Calcium central logged ratio and (D) Silica central logged ratio; (E) Diatom dissolution *F*_Index summary; (F) key diatom species (%), *Pantocsekiella ocellata*, *Lindavia comta*, *Nitzschia gracilis* and *Stephanodiscus parvus*, (G) C-IT reconstruction (°C, uncertainty of ± 1°C, note lower resolution of samples for the C-IT reconstruction), (H) Pollen summary showing relative proportions (%) and absolute concentrations of woody (grey) vs herbaceous (black) taxa. Dashed blue lines highlight section

of poor varve preservation with red dashed line highlighting the start of a section where varves are interpolated. Grey banding highlights period of increased windiness documented in the diatom record.

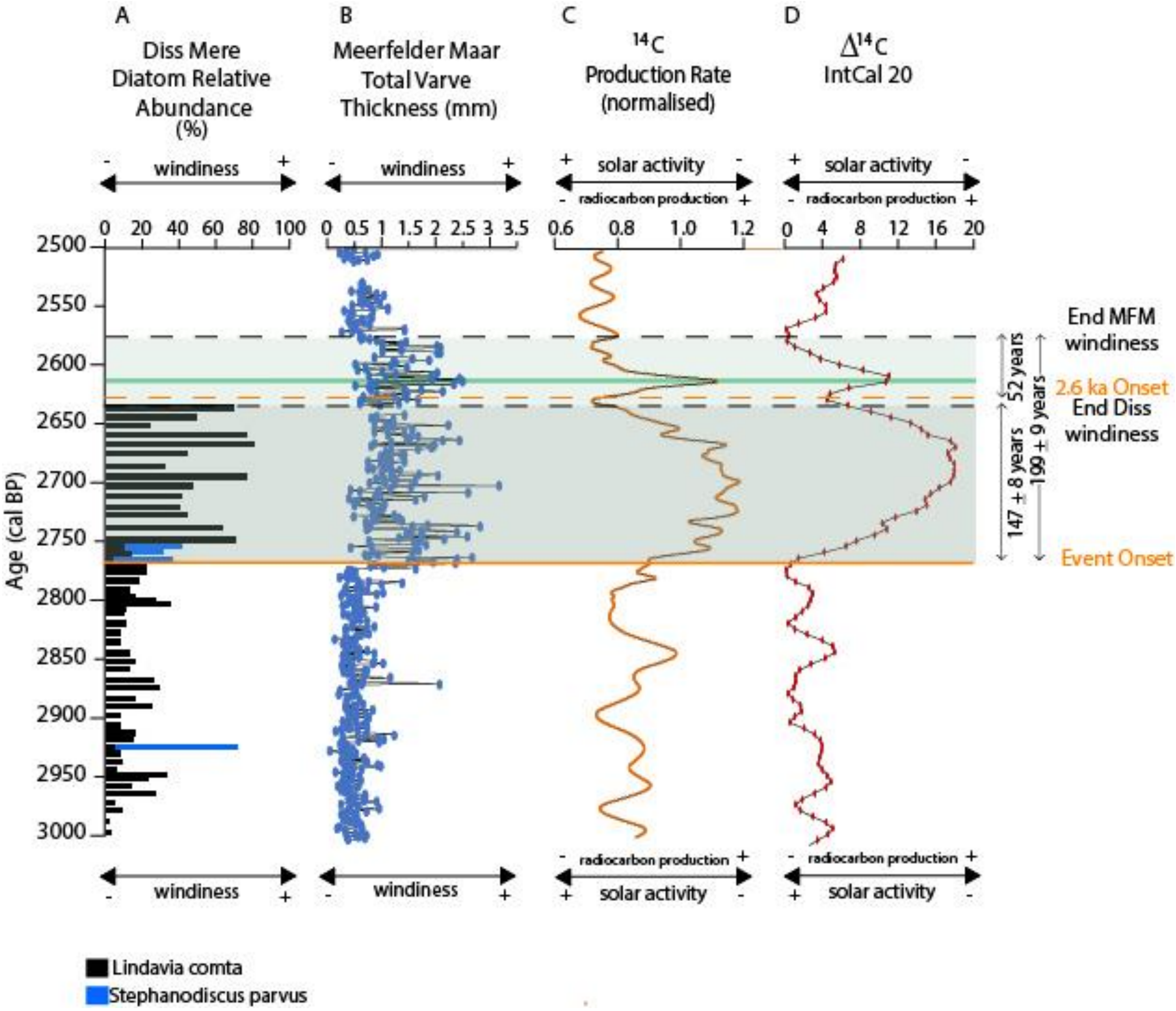

Fig. 3 Diss Mere and Meerfelder Maar Comparison. (a) Key wind influenced proxies at Diss Mere, *Lindavia comta*, *Stephanodiscus parvus* (relative abundances: %), (b) alongside the Meerfelder Maar varve thickness record (mm) (Martin-Puertas et al. 2012), (c) ^{14}C production rate (normalised (Muscheler et al. 2005) calculated from IntCal20 (Reimer et al. 2020)) and (d) 5-year resolution $\Delta^{14}C$ IntCal20 data (Reimer et al. 2020) for the 2500-3000 cal. BP time-period, which includes the effects of the carbon cycle leading to smoothening and delay of the peaks compared to ^{14}C production rate. Solid orange line marks the onset of the Homeric solar minimum, while the dashed orange line highlights the transition to the secondary lower amplitude solar minimum (Steinhilber et al. 2012). Coarse black dashed lines mark the end of intensified wind conditions at Diss Mere and Meerfelder Maar. Green line marks the position of the solar proton event at ~2610 cal. BP (O'Hare et al. 2019), which increases the annual normalised ^{14}C production rate (on top of the effect of the longer-term solar minimum). Durations on the intensified winds are shown. All datasets are presented on their independent chronologies.

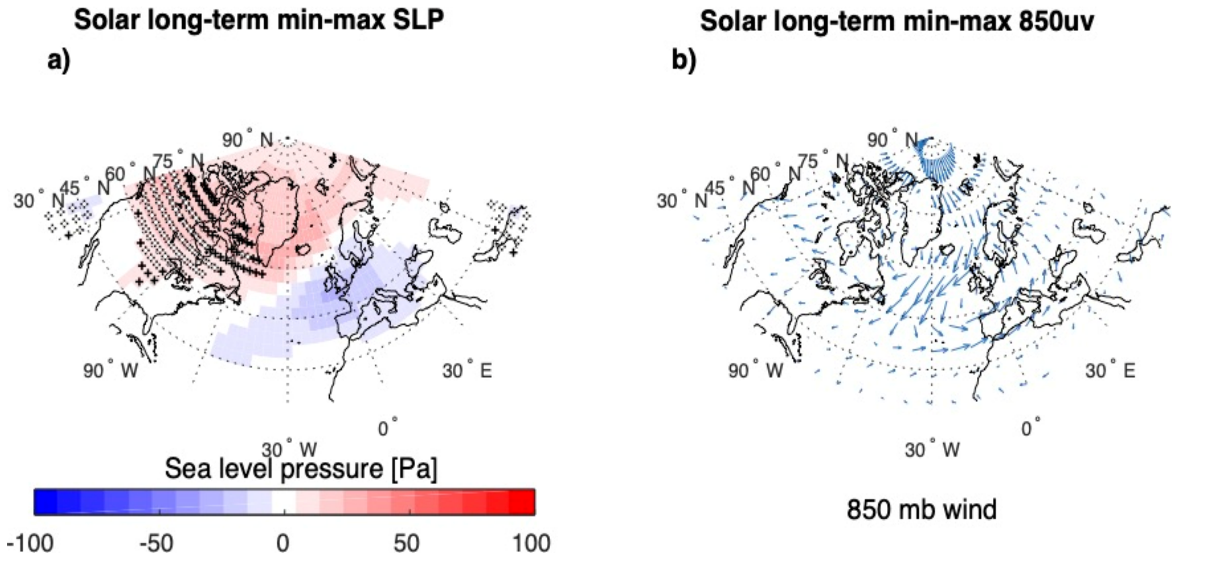

Fig. 4 Reconstructed atmospheric Sea Level Pressure (SLP) and the correlation to solar forcing (uv), derived from Sjolte al. (2018): (a) December, January, February (DJF) SLP anomalies (Pa) in response to long-term solar forcing (ultraviolet (uv)) (Brehm et al. 2021) (band-pass filtered for 60-500 year cycles). (b) corresponding figure to (a), but for the 850 mb wind. The white stippling (a) indicates significant anomalies $p < 0.05$, and black stippling indicates significant anomalies $p < 0.1$ (two-tailed Student's t test), and blue arrows (b) indicate predominant wind direction. The spatial resolution of the model is 3.75 x 3.75°.

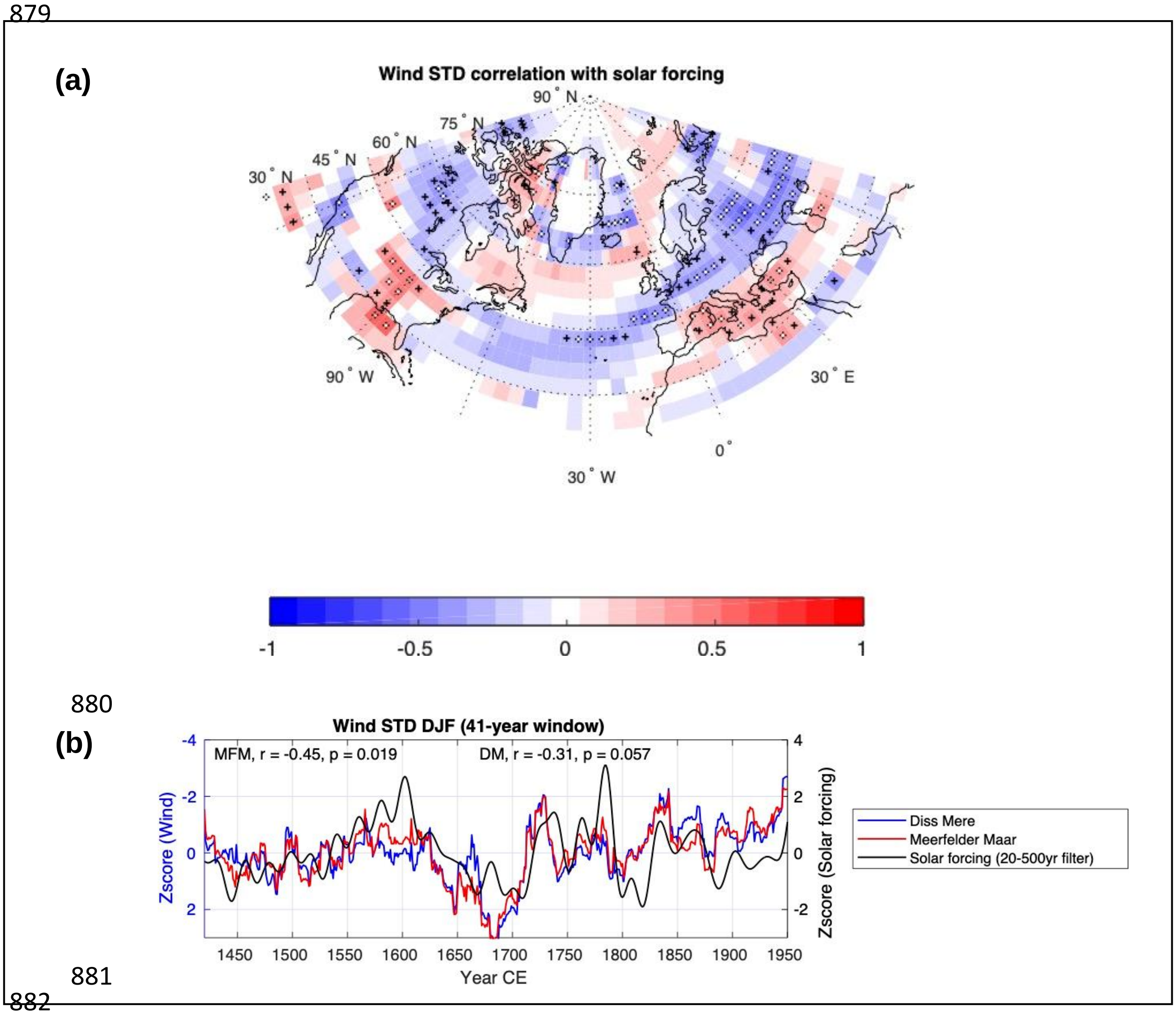

Fig 5 Wind STD Climate Reconstruction for 1400 – 1970 CE derived from Sjolte al. (2018): (a) Correlation between the moving 41-year standard deviation (STD) of the 850 mb wind and solar forcing (Brehm et al. 2021) (band-pass filtered for 60-500-year cycles) 1400 – 1970 CE. The white stippling indicates significant correlation $p < 0.05$, and black stippling indicates significant anomalies $p < 0.1$. (b) Time series of the moving 41-year STD of the 850 mb wind at Meerfelder Maar (MFM) and Diss Mere compared to solar forcing (Brehm et al. 2021). The significance is estimated taking autocorrelation into account (Ebisuzaki 1997)